High Frequency MoS_2 Nanomechanical Resonators

Jaesung Lee,[†,‡] Zenghui Wang,[†,‡] Keliang He,[§] Jie Shan,[§] and Philip X.-L. Feng[‡,*]

Departments of [‡]Electrical Engineering and Computer Science and [§]Physics, Case Western Reserve University, 10900 Euclid Avenue, Cleveland, Ohio 44106, United States. [†]These authors contributed equally.

ABSTRACT Molybdenum disulfide (MoS_2), a layered semiconducting material in transition metal dichalcogenides (TMDCs), as thin as a monolayer (consisting of a hexagonal plane of Mo atoms covalently bonded and sandwiched between two planes of S atoms, in a trigonal prismatic structure), has demonstrated unique properties and strong promises for emerging two-dimensional (2D) nanodevices. Here we report on the demonstration of movable and vibrating MoS_2 nanodevices, where MoS_2 diaphragms as thin as 6 nm (a stack of 9 monolayers) exhibit fundamental-mode nanomechanical resonances up to $f_0 \sim 60$ MHz in the very high frequency (VHF) band, and frequency-quality (Q) factor products up to $f_0 \times Q \sim 2 \times 10^{10}$Hz, all at room temperature. The experimental results from many devices with a wide range of thicknesses and lateral sizes, in combination with theoretical analysis, quantitatively elucidate the elastic transition regimes in these ultrathin MoS_2 nanomechanical resonators. We further delineate a roadmap for scaling MoS_2 2D resonators and transducers toward microwave frequencies. This study also opens up possibilities for new classes of vibratory devices to exploit strain- and dynamics-engineered ultrathin semiconducting 2D crystals.

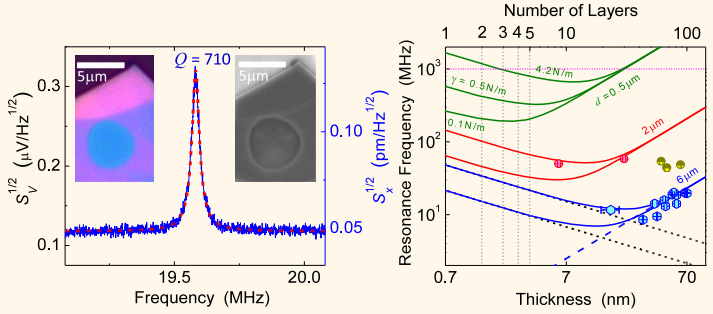

KEYWORDS: two-dimensional (2D) crystals · molybdenum disulfide (MoS_2) · nanoelectromechanical systems (NEMS) · resonators · thermomechanical noise · frequency scaling · displacement sensitivity

Actuating and sensing at the nanoscale are among the most important yet challenging functions in realizing new tools to interact with ultrasmall objects of interest. Such actuating and sensing functions often require harnessing mechanical degrees of freedom and exquisitely motion-coupled properties in nanostructures. Nanoelectromechanical systems (NEMS) based on atomically thin, two-dimensional (2D) crystals, such as graphene,[1−5] have recently shown attractive potential for novel actuators and sensors, owing to the ultralow weight and ultrahigh mechanical flexibility of these materials and other 2D attributes that are inaccessible in bulk.[1−7] While graphene, the early hallmark of 2D crystals, has been extensively studied for NEMS,[1−5] such explorations in 2D crystals beyond graphene with distinct electronic and optical properties are highly desirable.

Ultrathin crystals of transition metal dichalcogenides (TMDCs)[8,9] have emerged as a new class of 2D layered materials beyond graphene. Molybdenum disulfide (MoS_2), a prototype semiconducting TMDC, with a sizable bandgap and unique valley and spin properties,[10−13] has demonstrated remarkable promise for new electronic and optoelectronic applications.[8−17] In contrast to graphene being a semimetal, MoS_2 is a semiconductor with its electronic structure dependent on thickness and continuously on strain, as demonstrated experimentally.[10,11,18] 2D MoS_2 crystals also offer excellent mechanical properties,[18−20] similar to those of graphene.[1−7] In addition to its ultralow weight (areal density of $\rho_A = 3.3$fg/μm^2 for monolayer), 2D MoS_2 has exceptional strain limit ($\varepsilon_{int} \sim 10-20\%$)[18,19] and high elastic modulus ($E_Y \sim 0.2-0.3$TPa).[19,20] These properties suggest intriguing possibilities for innovating NEMS transducers where the mechanical properties of 2D MoS_2 are coupled to its band structure and other electronic and optoelectronic attributes (unavailable in graphene). However, motion-coupled MoS_2 nanodevices have not yet been explored, due to the difficulties not only in nanofabrication of movable

* Address correspondence to philip.feng@case.edu.

Received for review April 17, 2013 and accepted June 5, 2013.

Published online June 05, 2013
10.1021/nn4018872

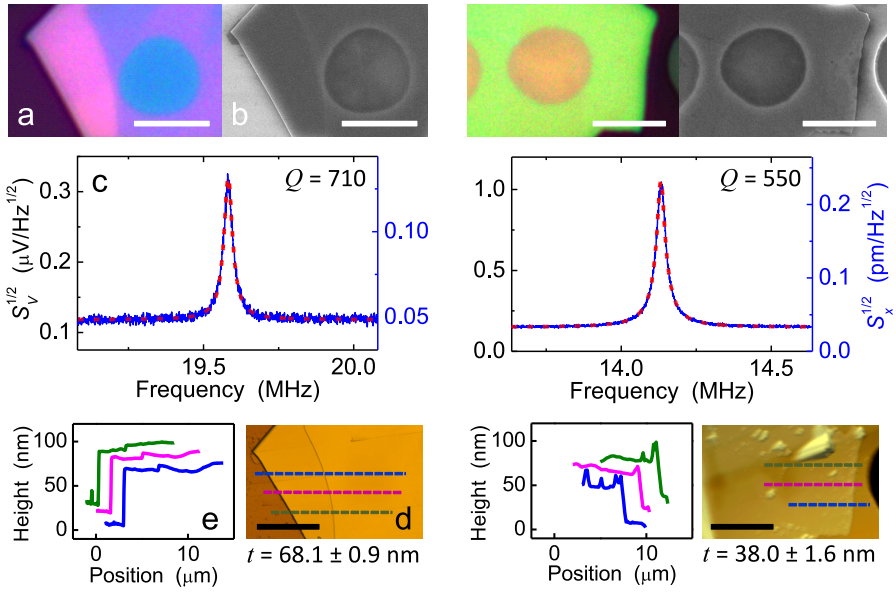

Figure 1. High frequency (HF) MoS_2 nanomechanical resonators and device characteristics. The left and right panels show data from two representative devices with different thicknesses. Shown in the same order within both panels: (a) Optical image; (b) SEM image; (c) Measured thermomechanical resonance (solid curve) and fit to a finite-*Q* harmonic resonator model (dashed curve); (d) AFM image (dashed lines indicate the approximate positions of height measurement traces); (e) Representative height measurement traces (offset for clarity), with colors corresponding to the dashed lines in (d). All scale bars are 5 μm.

devices, but also in detection of their vanishingly miniscule motions. In this work, we demonstrate MoS_2 NEMS resonators with resonances in the high and very high frequency (HF and VHF) bands, achieving displacement sensitivity of 30.2 fm/Hz$^{1/2}$, and with fundamental-mode frequency-quality factor product up to $f_0 \times Q \approx 2 \times 10^{10}$Hz, a figure of merit that surpasses values in graphene NEMS counterparts.[1−5] Combining experiment and analysis, we illustrate the important elastic regimes with scaling laws, which shed light on design and engineering of future devices toward microwave frequencies.

RESULTS AND DISCUSSION

Device Processing, Characterization, and Thermomechanical Resonance Measurement. We employ photolithography, wet etching, and micromechanical exfoliation to fabricate our prototype MoS_2 NEMS, which consist of exfoliated MoS_2 nanosheets covering predefined microtrenches on a SiO_2-on-Si substrate (see Methods). The thickness of each suspended MoS_2 diaphragm is initially estimated by examining its color and contrast in optical microscope. After all the resonance measurements that we describe below, the thickness and surface of each device is carefully examined using atomic force microscopy (AFM) and scanning electron microscopy (SEM).

Without external excitations, thermal fluctuation and dissipation processes dictate the devices to be in Brownian motions, manifested as thermomechanical modes of damped harmonic resonators, each with a frequency-domain displacement spectral density (see Supporting Information, S1)

$$S_{x,th}^{1/2}(\omega) = \left(\frac{4k_B T\omega_0}{M_{eff}Q}\cdot\frac{1}{(\omega^2-\omega_0^2)^2+\omega^2\omega_0^2/Q^2}\right)^{1/2} \quad (1)$$

Here k_B is the Boltzmann constant, M_{eff}, ω_0, and Q are the effective mass, angular resonance frequency, and quality factor of the mode, respectively. Given the structure and shape of our devices, the fundamental mode of the out-of-plane thermomechanical motions is the most salient. Thermomechanical motions are the minimal levels of motions that can be possibly measured from the devices, and set a fundamental limit for detection. We employ a specially engineered optical interferometry scheme that efficiently transduces motion into a voltage signal, $S_{v,th}^{1/2}(\omega) = \mathcal{R}(\omega)S_{x,th}^{1/2}(\omega)$ with $\mathcal{R}(\omega)$ being the transduction responsivity and with best motion sensitivities at the level of ~30 fm/Hz$^{1/2}$ (see Methods and Supporting Information, S1 and S6). This enables us to directly observe the intrinsic thermomechanical modes of the devices at room temperature, and for some devices, in both vacuum and ambient air.

High Frequency and Very High Frequency MoS_2 Nanomechanical Resonators. We first demonstrate high frequency nanomechanical resonators based on MoS_2 diaphragms of $d \sim 6$ μm in diameter, with thickness in the range of $t \approx 13-68$ nm (~20−97 layers). The left panel in Figure 1 shows the characteristics measured from a diaphragm with $d \approx 5.7$ μm and $t \approx 68.1$ nm. This device exhibits a fundamental mode resonance at $f_0 \equiv \omega_0/2\pi \approx 19.68$ MHz, with $Q \approx 710$ (Figure 1c) in moderate vacuum of pressure (p) ≈ 6 mTorr. This device makes an exquisite interferometric motion transducer with a displacement sensitivity (noise floor) of 49.5 fm/Hz$^{1/2}$ (see Supporting Information, S1). AFM measurements (Figure 1d,e)

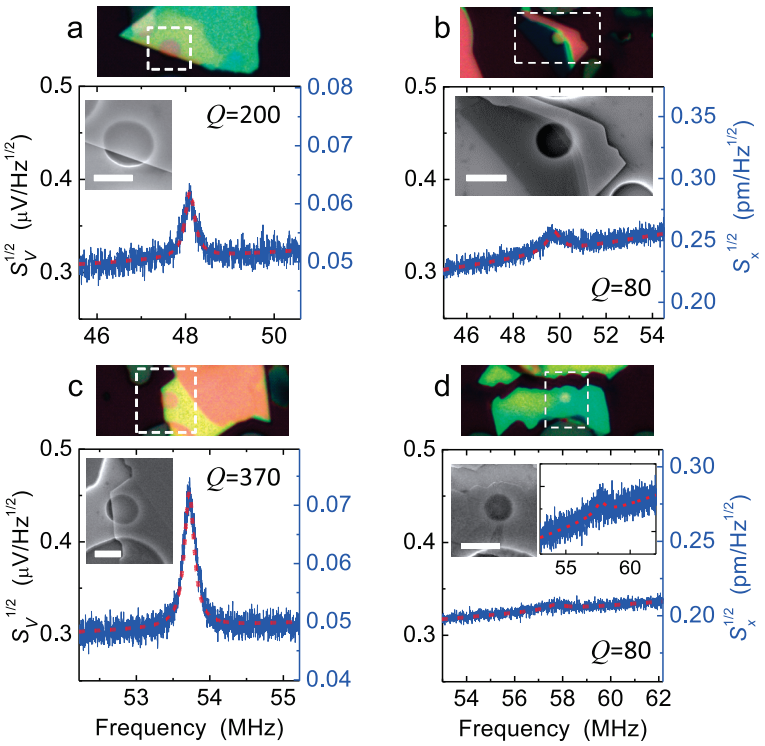

Figure 2. Very high frequency (VHF) thermomechanical resonances measured from smaller and thinner MoS_2 resonators. For each of the four devices, optical image, SEM image (corresponding to the dashed box in the optical image), and thermomechanical resonance are shown. The left axis denotes measured noise voltage spectral density, with the same scale in all four plots. The right axis is thermomechanical displacement spectral density, with individual scale depending on the characteristics of each device (thus, the interferometric transduction). Right inset in (d) is a zoom-in view of the same curve (rescaled the vertical axis). Device dimensions: (a) $d \approx 2.7$ μm, $t \approx 62.2$ nm (89 layers); (b) 1.9 μm, 6.1 nm (9 layers); (c) 2.5 μm, 43.0 nm (61 layers); (d) 1.5 μm, 27.2 nm (39 layers). All scale bars are 2 μm.

show thickness and surface morphological features. Right panel of Figure 1 shows data from a thinner device of similar size ($d \approx 5.5$ μm, $t \approx 38.0$ nm, ~54 layers) with $f_0 \approx 14.13$ MHz and $Q \approx 550$, and a remarkable displacement sensitivity of 33.5 fm/Hz$^{1/2}$.

We further explore smaller, thinner devices and demonstrate MoS_2 resonators in the VHF (30−300 MHz) band (Figure 2). The thinnest device (Figure 2b), only 9-layer-thick (see Supporting Information, S2 for details), makes a VHF resonator with $f_0 \approx 49.7$ MHz and $Q \approx 80$. We further note that these MoS_2 resonators are very robust; even incompletely covered devices (Figure 2a,c) operate at VHF with considerably high quality factors (Qs). These smaller circular diaphragms all make excellent interferometric motion transducers with displacement resolutions down to ~40−250 fm/Hz$^{1/2}$ in the 30−60 MHz band.

We summarize in Figure 3a,b the characteristics, including both the resonance frequencies (f_0 values) and the Qs of all the devices investigated, with various dimensions. It is clear (Figure 3a) that smaller diameters lead to higher frequencies. In both groups, thicker devices tend to attain higher Qs (Figure 3b), suggesting surface-related dissipations ($Q^{-1} \propto 1/t$, or the surface-to-volume ratio, $S/V \sim 1/t$) in these devices. This is in excellent agreement with the well-known thickness-dependent Qs in conventional MEMS/NEMS resonators that have high surface-to-volume ratios.[21,22]

We note that, in an earlier study on resonators made of graphene and very thin graphite,[1] no clear Q dependence on thickness was observed, which is in contrast with observations in this work and previous studies.[21,22] It could be that the surface-related dissipation in those graphene/graphite resonators might have been overshadowed by other stronger damping effects. While there are considerable varieties of device sizes and thicknesses, we can use a widely adopted figure of merit (FOM), $f_0 \times Q$ product, to evaluate device performance and compare the MoS_2 resonators in this work with recent graphene resonators.[1−5] The best FOM value achieved in our MoS_2 resonators is $f_0 \times Q \approx 2 \times 10^{10}$ Hz, which surpasses the highest $f_0 \times Q$ value in graphene devices reported to date, at room temperature and under similar experimental conditions.

We repeatedly observe that most of the thermomechanical resonances sustain even in ambient air. As shown in Figure 3d, Qs of ~500−100 in vacuum drop to ~10^{-1} in air, following a power law of $Q \propto p^{-1/2}$ in the range of $p \sim 1$−100 Torr, and then $Q \propto p^{-1}$ in the range of $p \sim 100$−1000 Torr. These measured air damping (Q dependence on pressure) characteristics of MoS_2 resonators are similar to the Q-pressure dependence measured in other membrane-structured MEMS/NEMS resonators.[23] Data in all other plots are measured at $p \approx 6$ mTorr and therefore are not compromised by air damping. In Q data from vacuum in all devices, besides the visible correlation

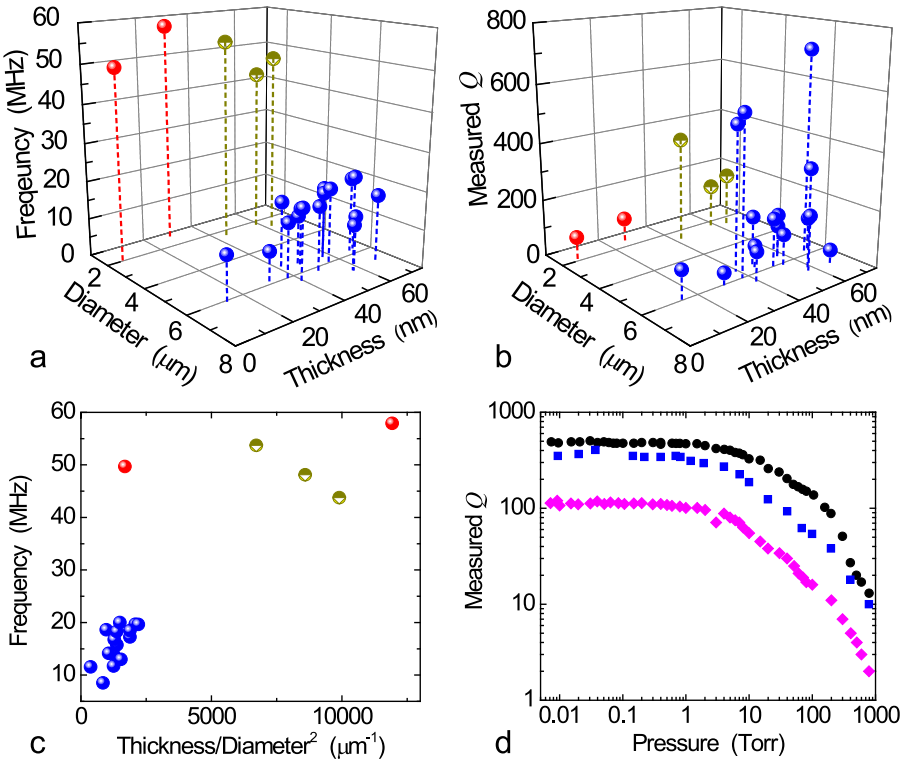

Figure 3. Performance of MoS_2 nanomechanical resonators. (a) Measured fundamental-mode resonance frequency, and (b) measured *Q* factor as functions of device dimensions. (c) Resonance frequency *vs* thickness over square of diameter (t/d^2). The blue and red symbols in a–c represent bigger and smaller devices, respectively. The divided-color symbols indicate devices based on incompletely covered microtrenches. (d) Measured *Q* dependence on pressure for different resonances. We have investigated >20 devices, see Supporting Information, S6, for a complete list of devices and their measured parameters.

to thickness (or $S/V \sim 1/t$), we observe no noticeable evidence suggesting dominant clamping losses (dependent on aspect ratio, *i.e.*, length-to-thickness or diameter-to-thickness ratio)[24,25] or other mechanisms.

Theoretical Analysis of Elastic Transition Regime and Frequency Scaling. To gain insight and quantitative understandings of the device frequency scaling, we perform analytical modeling. For vibrations of clamped MoS_2 diaphragms with both flexural rigidity $D = Et^3/[12(1-\nu^2)]$ (ν being the Poisson ratio) and tension γ (N/m, as in surface tension), we determine the fundamental-mode resonance frequency to be[26,27]

$$f_0 = \left(\frac{kd}{4\pi}\right)\sqrt{\frac{16D}{\rho d^4}\left[\left(\frac{kd}{2}\right)^2 + \frac{\gamma d^2}{4D}\right]} \qquad (2)$$

where ρ is the areal mass density and k is a modal parameter that is determined numerically (see Supporting Information, S3). In the tension-dominant limit ($\gamma d^2/D \to \infty$), eq 2 converges into the membrane model, while in the modulus-dominant limit ($\gamma d^2/D \to 0$) it approaches the plate model. These asymptotic characteristics are clearly demonstrated in Figure 4, with scaling of f_0 upon varying device thickness. This leads to the *quantitative* determination of a "crossover" transition regime at intermediate thicknesses for any given diameter and tension level. Experimental data from

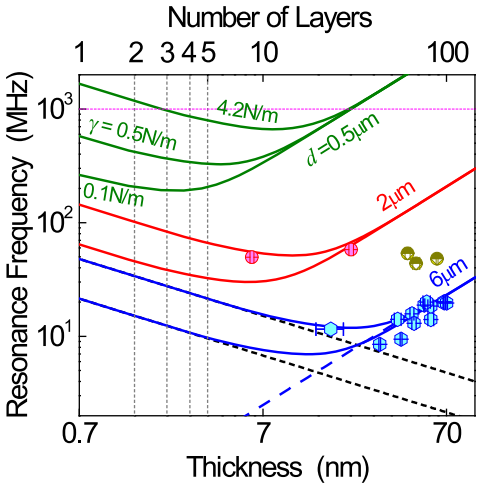

Figure 4. Elucidating elastic transition from the "plate" limit to the "membrane" limit in very thin MoS_2 resonators: (solid curves) calculated resonance frequency *vs* device thickness for three different device diameters, each with 0.1 and 0.5 N/m tension (except in the top curve family where we show an additional tension of 4.2 N/m, corresponding to 3% strain in monolayer); (black dashed lines) 6 μm ideal membranes (eq S12) under 0.1 and 0.5 N/m tension; (blue dashed line) 6 μm ideal plate (eq S13); (blue hexagons) measured devices with large diameter (~6 μm); (red circles) small diameter (~2 μm) devices. Circles with divided colors denote slightly larger (~2.5 μm) devices with less than complete coverage (as shown in Figure 2). Vertical dotted lines mark the thicknesses of 2–5 layers of MoS_2.

larger-diameter ($d \sim 6\ \mu$m) devices agree well with the 6 μm curves, and data from smaller-diameter ($d \sim 2\ \mu$m) devices match the 2 μm curves. Data from slightly larger ($d \sim 2.5\ \mu$m) and incomplete diaphragms (see SEM images in Figure 2 for examples) fall in between the data from the above two groups.

Comparing our experimental and analytical results, we find that thicker devices essentially operate in the plate limit, where f_0 is determined by the device dimensions and shows little dependence on tension. This is also evident in Figure 3c where data from larger devices ($d \sim 6\ \mu$m) appear to follow the trend of $f_0 \propto t/d^2$ for ideal plates. In contrast, our thinnest devices operate in the transition regime and approach the membrane limit. From these results we estimate a tension level of $\gamma \approx 0.3-0.5$ N/m in these devices, consistent with values obtained in static nanoindentation tests of mechanically exfoliated MoS_2.[19,20] This value is also comparable with that found in exfoliated graphene,[6] suggesting similarity in the exfoliation processes of both materials. We note that these tension values correspond to strains of only $\varepsilon \approx 0.01-0.04\%$, which are $\sim$250−2000 times lower than the intrinsic strain limit ($\sim$10−20%).[18,19]

Our analysis indicates that ultrathin devices (e.g., below five monolayers, vertical dashed lines in Figure 4) will operate in the membrane limit and attain great tunability *via* tension. Importantly, here we clearly demonstrate that for $d \sim 2-6\ \mu$m or larger, devices thinner than 10−20 layers are already well in the membrane regime. For $d < 1\ \mu$m, only few-layer devices behave as membranes. Figure 4 also provides the design guidelines and scaling laws: reducing the lateral dimension and engineering high tension are both effective toward scaling up the resonance frequency. For instance, for $d = 0.5\ \mu$m (the green curves in Figure 4), resonators with $f_0 = 1$ GHz can be achieved in both asymptotic regimes, by trading thickness *versus* tension. In particular, even a moderate tension of $\gamma \approx 4.2$ N/m (strain $\varepsilon \approx 1.5\%$ for bilayer and $\varepsilon \approx 3\%$ for monolayer) leads to $f_0 > 1$ GHz for $d = 0.5\ \mu$m devices with less than three layers (Figure 4).

CONCLUSIONS

In conclusion, we have demonstrated a new type of nanomechanical resonators vibrating in the HF and VHF bands based on suspended 2D MoS_2 crystals. These MoS_2 devices demonstrate robust resonances with high Qs and naturally make motion transducers exhibiting exceptional displacement sensitivities approaching 30 fm/Hz$^{1/2}$ at room temperature. A figure of merit $f_0 \times Q \approx 2 \times 10^{10}$ Hz is achieved at room temperature, among the highest in known nanomechanical resonators based on 2D materials including graphene. Our study unambiguously identifies the transition between the "plate" and "membrane" regimes and establishes quantitative design guidelines and scaling laws for engineering future generations of MoS_2 NEMS and ultrasensitive 2D resonant transducers. As thermomechanical fluctuations represent a fundamental noise floor, the thermomechanical resonant characteristics measured from the MoS_2 devices may provide important information for future engineering of MoS_2 resonant NEMS, where achieving large dynamic range[28] and matching to intrinsic noise floor are important. Examples include low-noise feedback oscillators,[29] noise thermometry,[30] and signal transduction near the quantum limit.[31] Furthermore, the demonstration of very high frequency MoS_2 nanomechanical resonators with frequency scaling capability enables a 2D semiconducting NEMS platform for a number of exciting future experiments and device technologies, such as coupling dynamical strains and resonant motions into MoS_2 field effect transistors[15−17] and optoelectronic devices,[9,32] exploring spin interactions with MoS_2 NEMS resonators for quantum information processing,[33] and engineering vibratory and flexible devices toward fully exploiting the very high intrinsic strain limits[18,19] promised by ultrathin MoS_2 structures.

METHODS

Device Fabrication. MoS_2 nanomechanical resonators are fabricated by exfoliating MoS_2 nanosheets onto prefabricated device structures. First, circular microtrenches of different sizes are patterned onto a silicon (Si) wafer covered with 290 nm of thermal oxide (SiO_2) using photolithography followed by buffered oxide etch (BOE). The etch time is chosen such that the flat Si surface is exposed. Then MoS_2 nanosheets are exfoliated onto this structured substrate. We note that the yield for making suspended MoS_2 devices with fully covered microtrenches is much lower than for making graphene devices with similar geometries, especially for thinner (mono- and few-layer) devices. Suspended MoS_2 sheets covering microtrenches are then identified under an optical microscope (Olympus MX50) with a 50× objective, where all the optical images are taken.

Thermomechanical Resonance Measurement. Undriven Brownian motions of MoS_2 nanomechanical resonators are measured with a custom-built laser interferometry system (see Supporting Information, S1, for details). A He−Ne laser (632.8 nm) is focused onto the suspended MoS_2 diaphragms using a 50× microscope objective, with a spot size of $\sim$1 μm. We apply a laser power of $\sim$100 μW−700 μW onto the device which assures good optical signal and does not exhibit measurable heating (see Supporting Information, S4). Optical interferometric readout of the MoS_2 device motion is accomplished by detecting the motion-modulated interference between the reflections from the MoS_2 diaphragm−vacuum interfaces and the underneath vacuum−Si interface. We have specially engineered our system to achieve pm/Hz$^{1/2}$ to fm/Hz$^{1/2}$ displacement sensitivities for various devices by exploiting latest advances and techniques in such schemes.[34−36] The optical detection scheme and settings are carefully tuned to remain identical during the experiments. The vacuum chamber is maintained under moderate vacuum ($\sim$6 mTorr), except during characterization of air damping, when the pressure is regulated and varied between vacuum and atmospheric pressure (760 Torr). Throughout the pressure dependence measurements we observe no evidence of bulging effect due to trapped air underneath MoS_2 diaphragms

(see Supporting Information, S5). Thermomechanical noise spectral density is recorded with a spectrum analyzer (Agilent E4440A).

Scanning Electron Microscopy (SEM). SEM images are taken inside an FEI Nova NanoLab 200 field-emission SEM, using an Everhart-Thornley detector (ETD) for detecting secondary electrons at an acceleration voltage of 10 kV.

Atomic Force Microscopy (AFM). AFM images are taken with an Agilent N9610A AFM using tapping mode. To measure the thickness of each device, multiple traces are extracted from each scan, from which the thickness value and uncertainty are determined (see Supporting Information, S2).

Conflict of Interest: The authors declare no competing financial interest.

Acknowledgment. This work was supported by Case School of Engineering and the National Science Foundation (Grant No. DMR-0907477). We are also grateful to a T. Keith Glennan Fellowship and the Swagelok Center for Surface Analysis of Materials (SCSAM) at Case Western Reserve University.

Supporting Information Available: Additional technical details. This material is available free of charge *via* the Internet at http://pubs.acs.org.

REFERENCES AND NOTES

1. Bunch, J. S.; van der Zande, A. M.; Verbridge, S. S.; Frank, I. M.; Tanenbaum, D. M.; Parpia, J. M.; Craighead, H. G.; McEuen, P. L. Electromechanical Resonators from Graphene Sheets. *Science* **2007**, *315*, 490–493.
2. Chen, C. Y.; Rosenblatt, S.; Bolotin, K. I.; Kalb, W.; Kim, P.; Kymissis, I.; Stormer, H. L.; Heinz, T. F.; Hone, J. Performance of Monolayer Graphene Nanomechanical Resonators with Electrical Readout. *Nat. Nanotechnol.* **2009**, *4*, 861–867.
3. van der Zande, A. M.; Barton, R. A.; Alden, J. S.; Ruiz-Vargas, C. S.; Whitney, W. S.; Pham, P. H. Q.; Park, J. W.; Parpia, J. M.; Craighead, H. G.; McEuen, P. L. Large-Scale Arrays of Single-Layer Graphene Resonators. *Nano Lett.* **2010**, *10*, 4869–4873.
4. Eichler, A.; Moser, J.; Chaste, J.; Zdrojek, M.; Wilson-Rae, I.; Bachtold, A. Nonlinear Damping in Mechanical Resonators Made from Carbon Nanotubes and Graphene. *Nat. Nanotechnol.* **2011**, *6*, 339–342.
5. Barton, R. A.; Parpia, J.; Craighead, H. G. Fabrication and Performance of Graphene Nanoelectromechanical Systems. *J. Vac. Sci. Technol., B* **2011**, *29*, 050801.
6. Lee, C.; Wei, X.; Kysar, J. W.; Hone, J. Measurement of the Elastic Properties and Intrinsic Strength of Monolayer Graphene. *Science* **2008**, *321*, 385–388.
7. Lee, C.; Li, Q. Y.; Kalb, W.; Liu, X.-Z.; Berger, H.; Carpick, R. W.; Hone, J. Frictional Characteristics of Atomically Thin Sheets. *Science* **2010**, *328*, 76–80.
8. Novoselov, K. S.; Jiang, D.; Schedin, F.; Booth, T. J.; Khotkevich, V. V.; Morozov, S. V.; Geim, A. K. Two-Dimensional Atomic Crystals. *Proc. Natl. Acad. Sci. U.S.A.* **2005**, *102*, 10451–10453.
9. Wang, Q. H.; Kalantar-Zadeh, K.; Kis, A.; Coleman, J. N.; Strano, M. S. Electronics and Optoelectronics of Two-Dimensional Transition Metal Dichalcogenides. *Nat. Nanotechnol.* **2012**, *7*, 699–712.
10. Mak, K. F.; Lee, C.; Hone, J.; Shan, J.; Heinz, T. F. Atomically Thin MoS_2: A New Direct-Gap Semiconductor. *Phys. Rev. Lett.* **2010**, *105*, 136805.
11. Splendiani, A.; Sun, L.; Zhang, Y. B.; Li, T. S.; Kim, J. H.; Chim, C.-Y.; Galli, G.; Wang, F. Emerging Photoluminescence in Monolayer MoS_2. *Nano Lett.* **2010**, *10*, 1271–1275.
12. Zeng, H. L.; Dai, J .F.; Yao, W.; Xiao, D.; Cui, X. D. Valley Polarization in MoS_2 Monolayers by Optical Pumping. *Nat. Nanotechnol.* **2012**, *7*, 490–493.
13. Mak, K. F.; He, K. L.; Shan, J.; Heinz, T. F. Control of Valley Polarization in Monolayer MoS_2 by Optical Helicity. *Nat. Nanotechnol.* **2012**, *7*, 494–498.
14. Lee, C.; Yan, H.; Brus, L. E.; Heinz, T. F.; Hone, J.; Ryu, S. Anomalous Lattice Vibrations of Single- and Few-Layer MoS_2. *ACS Nano* **2010**, *4*, 2695–2700.
15. Radisvljevic, B.; Radenovic, A.; Brivio, J.; Giacometti, V.; Kis, A. Single-Layer MoS_2 Transistors. *Nat. Nanotechnol.* **2011**, *6*, 147–150.
16. Liu, H.; Ye, P. D. MoS_2 Dual-Gate MOSFET with Atomic-Layer Deposited Al_2O_3 as Top-Gate Dielectric. *IEEE Electron Device Lett.* **2012**, *33*, 546–548.
17. Wang, H.; Yu, L. L.; Lee, Y.-H.; Shi, Y. M.; Hsu, A.; Chin, M. L.; Li, L.-J.; Dubey, M.; Kong, J.; Palacios, T. Integrated Circuits Based on Bilayer MoS_2 Transistors. *Nano Lett.* **2012**, *12*, 4674–4680.
18. He, K.; Poole, C.; Mak, K. F.; Shan, J. Experimental Demonstration of Continuous Electronic Structure Tuning *via* Strain in Atomically Thin MoS_2. *Nano Lett.* **2013**, DOI: 10.1021/nl4013166, and references therein.
19. Bertolazzi, S.; Brivio, J.; Kis, A. Stretching and Breaking of Ultrathin MoS_2. *ACS Nano* **2011**, *5*, 9703–9709.
20. Castellanos-Gomez, A.; Poot, M.; Steele, G. A.; van der Zant, H. S. J.; Agraït, N.; Rubio-Bollinger, G. Elastic Properties of Freely Suspended MoS_2 Nanosheets. *Adv. Mater.* **2012**, *24*, 772–775.
21. Yasumura, K. Y.; Stowe, T. D.; Chow, E. M.; Pfafman, T.; Kenny, T. W.; Stipe, B. C.; Rugar, D. Quality Factors in Micron- and Submicron-Thick Cantilevers. *J. Microelectromech. Syst.* **1999**, *9*, 117–125.
22. Yang, J. L.; Ono, T.; Esashi, M. Energy Dissipation in Submicronmeter Thick Single-Crystal Silicon Cantilevers. *J. Microelectromech. Syst.* **2002**, *11*, 775–783.
23. Southworth, D. R.; Craighead, H. G.; Parpia, J. M. Pressure Dependent Resonant Frequency of Micromechanical Drumhead Resonators. *Appl. Phys. Lett.* **2009**, *94*, 213506.
24. Cross, M. C.; Lifshitz, R. Elastic Wave Transmission at an Abrupt Junction in a Thin Plate, with Application to Heat Transport and Vibrations in Mesoscopic Systems. *Phys. Rev. B* **2001**, *64*, 085324.
25. Feng, X. L.; He, R.; Yang, P.; Roukes, M. L. Very High Frequency Silicon Nanowire Electromechanical Resonators. *Nano Lett.* **2007**, *7*, 1953–1959.
26. Wah, T. Vibration of Circular Plates. *J. Acoust. Soc. Am.* **1962**, *34*, 275–281.
27. Suzuki, H.; Yamaguchi, N.; Izumi, H. Theoretical and Experimental Studies on the Resonance Frequencies of a Stretched Circular Plate: Application to Japanese Drum Diaphragms. *Acoust. Sci. Technol.* **2009**, *30*, 348–354.
28. Postma, H. W. C.; Kozinsky, I.; Husain, A.; Roukes, M. L. Dynamic Range of Nanotube- and Nanowire-Based Electromechanical Systems. *Appl. Phys. Lett.* **2005**, *86*, 223105.
29. Feng, X. L.; White, C. J.; Hajimiri, A.; Roukes, M. L. A Self-Sustaining Ultrahigh-Frequency Nanoelectromechanical Oscillator. *Nat. Nanotechnol.* **2008**, *3*, 342–346.
30. Poggio, M.; Degen, C. L.; Mamin, H. J.; Rugar, D. Feedback Cooling of a Cantilever's Fundamental Mode below 5mK. *Phys. Phys. Lett.* **2007**, *99*, 017201.
31. Thompson, J. D.; Zwickl, B. M.; Jayich, A. M.; Marquardt, F.; Girvin, S. M.; Harris, J. G. E. Strong Dispersive Coupling of a High-Finesse Cavity to a Micromechanical Membrane. *Nature* **2008**, *452*, 72–75.
32. Sundaram, R. S.; Engel, M.; Lombardo, A.; Krupke, R.; Ferrari, A. C.; Avouris, Ph.; Steiner, M. Electroluminescence in Single Layer MoS_2. *Nano Lett.* **2013**, 1310.1021/nl400516a.
33. Rabl, P.; Kolkowitz, S. J.; Koppens, F. H. L.; Harris, J. G. E.; Zoller, P.; Lukin, M. D. A Quantum Spin Transducer Based on Nanoelectromechancial Resonator Arrays. *Nat. Phys.* **2010**, *6*, 602–608.
34. Karabacak, D.; Kouh, T.; Ekinci, K. L. Analysis of Optical Interferometric Displacement Detection in Nanoelectromechanical Systems. *J. Appl. Phys.* **2005**, *98*, 124309.
35. Karabalin, R. K.; Matheny, M. H.; Feng, X. L.; Defay, E.; Le Rhun, G.; Marcoux, C.; Hentz, S.; Andreucci, P.; Roukes, M. L. Piezoelectric Nanoelectromechanical Resonators Based on Aluminum Nitride Thin Films. *Appl. Phys. Lett.* **2009**, *95*, 103111.
36. Hiebert, W. K.; Vick, D.; Sauer, V.; Freeman, M. R. Optical Interferometric Displacement Calibration and Thermomechanical Noise Detection in Bulk Focused Ion Beam-Fabricated Nanoelectromechanical Systems. *J. Micromech. Microeng.* **2010**, *20*, 115038.